Chlorophyll *a* Behavior in Aqueous Solvents: Formation of Nanoscale Self-Assembled Complexes

Angela Agostiano,*,†,‡ Pinalysa Cosma,†,‡ Massimo Trotta,‡ Luigi Monsù-Scolaro,§ and Norberto Micali||

Dipartimento di Chimica, Università di Bari and Istituto per i Processi Chimico-Fisici−IPCF-CNR Bari, Via Orabona, 4-70126 Bari, Italy, Dipartimento di Chimica Inorganica, Chimica Analitica e Chimica Fisica and ISMN-CNR, Sezione di Messina and INFM, Unità di Messina, Salita Sperone, 31-98166 Vill. S. Agata, Messina Italy, and Istituto per i Processi Chimico-Fisici, IPCF-CNR Messina, Via La Farina, 237-98123 Messina, Italy

Received: June 26, 2002; In Final Form: October 8, 2002

In this paper, the Chlorophyll *a* aggregation behavior is investigated in relation to the nature of the organic solvent, the composition of aqueous mixtures with different organic solvents, and the pigment concentration. Because of the complexity of the system under investigation and the number of parameters that can influence the Chlorophyll *a* aggregation processes, the data relative to the physicochemical characterization of the species will be discussed in three sessions, corresponding to different ranges of the solvent composition. Chlorophyll *a* behavior is discussed when present mainly as a monomer, as a polymer or as a "micellar" species, respectively. Particular attention is devoted to the pigment response in the water rich region, where the solvent behaves almost as pure water and the aggregation processes are essentially driven by hydrophobic interactions. The overall data above-reported are consistent with the formation of spherical-shaped aggregates of Chlorophyll *a* (of pheophytin *a*) molecules in which the phytil chains are segregated in the inner part, thus fostering the pigments to expose the macrocyclic heads toward the bulk water solvent. Besides optical techniques (UV−vis, fluorescence, and circular dichroism) used to investigate the spectral properties of the chlorophyll, the aggregation state is investigated by resonance and dynamic light scattering, nuclear magnetic resonance self-diffusion, transmission electron microscopy, and adsorption-stripping cyclic voltammetry.

Introduction

Chlorophyll *a* (Chl *a*)[1] is the main pigment involved in the photosynthetic process in higher plants and algae,[24,53] and it belongs to the larger class of chlorophylls present in all photosynthetic organisms. Chl *a* plays two fundamental roles in different membrane-bound enzymatic complexes: it acts as antennae excitons[23,64] in the light-harvesting complexes collecting and funneling light and as an electron carrier in the reaction centers, vectorially transferring electrons across the photosynthetic membrane.[31,32,58.]

The ability to perform such different mechanisms in vivo can be mainly ascribed to its molecular interactions within the proteic environment. These interactions involve the central Mg atom of the tetrapyrrole macrocycle, the carbonyl groups at C-131, C-13,[3] and C-17,[3] and the 17[3]-exo group (mostly phytol), which is relevant not only for the hydrophobicity of the molecule but also for the specific interactions in the pigment aggregation.[3,4,43,54] As result of such interactions, the absorption spectra of Chl *a* in vivo show a bathochromic shift when compared to that of the pigment dissolved in organic solvent. The evident relevance of the pigment ability to mutate physicochemical properties upon aggregation has induced several laboratories to investigate the conditions at which long wavelength-absorbing forms of chlorophyll can be formed in vitro, in polar and nonpolar solvents and in a series of membrane mimetic systems.[2,13,19,44,56,62] A large variety of techniques,[1,14,18,20,26,41,66] from electrochemistry to optical and magnetic spectroscopies, from mass spectrometry, light scattering, and microscopy to photochemistry, have been used to elucidate structures and properties of Chl *a* aggregates. In our laboratory, particular attention has been focused on a novel aggregate absorbing at around 713 nm, formed in the water rich region of a water−acetonitrile (ACN) mixture. For such aggregates, a structure is supposed in which the chlorophyll phytil chains, anchored by hydrophobic interactions in the inside of a "micellelike" aggregate, force the macrocycles to be displayed toward the bulk water.[24]

The aim of this paper is to further characterize Chl *a* behavior in relation to the organic solvent nature, the composition of the aqueous mixtures, and the pigment concentration. Particular attention will be devoted to the pigment response in the water rich region, where the solvent behaves almost as pure water and the aggregation processes are essentially driven by hydrophobic interactions. Besides optical techniques (UV−vis, fluorescence, and circular dichroism (CD)), employed to investigate the spectral properties of Chl *a*, the aggregation state is investigated by resonance light scattering (RLS) and dynamic light scattering (DLS), NMR self-diffusion, transmission electron microscopy (TEM), and adsorption-stripping cyclic voltammetry (ASCV).

* To whom correspondence should be addressed.
† Università di Bari.
‡ IPCF-CNR Bari.
§ Università di Messina.
|| IPCF-CNR Messina.

10.1021/jp026385k CCC: $22.00
Published on Web 11/14/2002

Material and Methods

Chl *a* was extracted from fresh spinach leaves and purified according to a previously published method.[13,14,66] Stock solutions in wet *n*-pentane were stored in the dark at −20 °C under a N_2 atmosphere. The purity and concentration of the samples were routinely checked by UV−vis spectroscopy in ether solution.[60] *N*,*N*-Dimethylformamide (DMF), ACN, acetone, methanol (MeOH), and ethanol (EtOH) from Fluka or Aldrich were distilled and used to solubilize the chlorophyll. Proper amounts of these solutions were injected in doubly distilled water to realize solutions of the opportune composition. Chl *a* concentration in the different organic solvents was checked by UV−vis spectroscopy using the characteristic Q_y-transition extinction coefficients.[57] Absorption spectra of samples were recorded on a Cary 3 Varian spectrophotometer. A nonlinear curve-fitting procedure of the UV−vis absorption spectra was performed by using the commercial software PeakFit (Jandel Scientific release 3.0) based on the Levenberg−Marquardt algorithm. Absorption peaks were initially graphically fitted with a Gaussian function, and the final numerical fitting procedure ended when the minimum value for the square of the residual (χ^2) was reached. Deconvolution of spectra recorded in Chl *a* solutions with the same mole fraction was performed keeping the peak positions and their full width at half-height (fwhh) constant for all investigated concentrations. The fitting data presented in the paper always exceeded $r^2 = 0.998$. The temperature of the cuvette holder was kept constant by a thermostatic bath within 0.1 °C.

Fluorescence and RLS spectra were performed on a Perkin-Elmer LS-5 spectrofluorimeter equipped with a chart recorder. RLS spectra were recorded with an excitation neutral density filter with 6% of transmittance. CD spectra were acquired on a JASCO J-500 spectropolarimeter. DLS experiments were performed by collecting the scattered light through optical fibers matched with a digital Hamamatsu R942 photomultiplier cooled at −30 °C. The signal was sent to a Malvern 4700 submicron particle analyzer system (eight parallel correlators at different sampling times) and the intensity−intensity correlation function $g^2(\tau)$ was measured in the time range 10 μs $\leq \tau \leq$ 1 s, using a typical acquisition time of 200 s. The exciting light source was a Spectra Physics Nd:YAG laser model Millennia II (0.3 W).

The adsorptive cathodic-stripping voltammetry was performed using a PAR 174A polarograph interfaced with an AMEL Plotter adapter/converter. A hanging drop mercury electrode (HDME, Metrohm EA. 290/1) with a drop surface of 1.39 ± 0.02 mm^2 was used as the working electrode. Voltammograms were recorded after 1 min of adsorption at fixed potential (−200 mV vs SCE) on the drop. The sample temperature was kept at 20 °C.

Self-diffusion coefficients of organic solvent were determined using Fourier transform−pulsed gradient spin−echo (FT-PGSE) on a Tesla BS 587 A 80 MHz spectrometer equipped with a pulsed field gradient unity (Stelar) and controlled by using HROCH software. A Stejskal−Tanner sequence, classical spin−echo sequence (90° τ−180° τ) modified with two rectangular field gradient pulses of δ duration separated by a time interval Δ, was used.[4] The echo amplitudes were analyzed by nonlinear fitting procedures. The sample temperature was kept at 298 ± 0.3 K using a variable temperature control unit of the spectrometer. The TEM characterization was performed observing the samples at 100 kV under a PHYLIPS 4007 TEM.

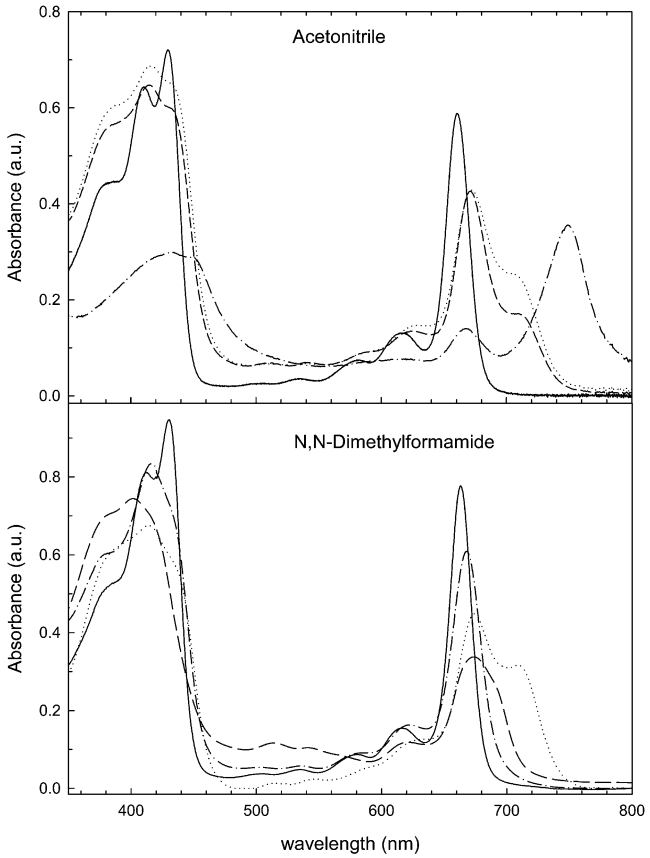

Figure 1. Absorption spectra of 7×10^{-6} M Chl *a* solution in ACN−water (upper panel) and DMF−water (lower panel) binary mixtures: (—) pure solvent; (− · − · −) 30% solvent in water; (− − −) 10% solvent in water; (· · ·) 1% solvent in water.

Results and Discussion

In Figure 1, the absorption spectra of Chl *a* in DMF/H_2O and ACN/H_2O binary mixtures are reported for solutions whose content in organic solvent ranges between 100 and 1%. The spectroscopic behavior of the pigment is strongly effected by both the nature and the amount of the organic solvent in solution. In DMF, monomer Chl *a* remains the only species present even in the presence of a large amount of water. A small bathochromic shift of the red peak along with a more relevant change in the peak shape in the blue region of the spectra suggest a change in the solvation of the macrocycle.[5,15] The increase of the binary mixture water content up to 99% results in the appearance of a shoulder associated to a new species of Chl *a* aggregate whose absorption maximum, from the deconvolution procedures, is around 713 nm (from now on called S713). In ACN, the S713 species is already present in solutions containing 10% of the organic solvent, and higher water content causes only the growth of the peak intensity as compared to the monomer one. Another relevant difference in the chlorophyll aggregation behavior in the two solvents is related to the formation of the polymer species, absorbing at 745 nm, in ACN for water content in solution ranging between 70 and 90%. No evidence of such a species was found in the DMF−water mixture over the entire range of solvent compositions and Chl *a* concentrations explored.

Because of the complexity of the system under investigation and the number of parameters that can influence the Chl *a* aggregation processes, the data relative to the physicochemical characterization of the species will be discussed in three sections, corresponding to different ranges of the solvent composition in

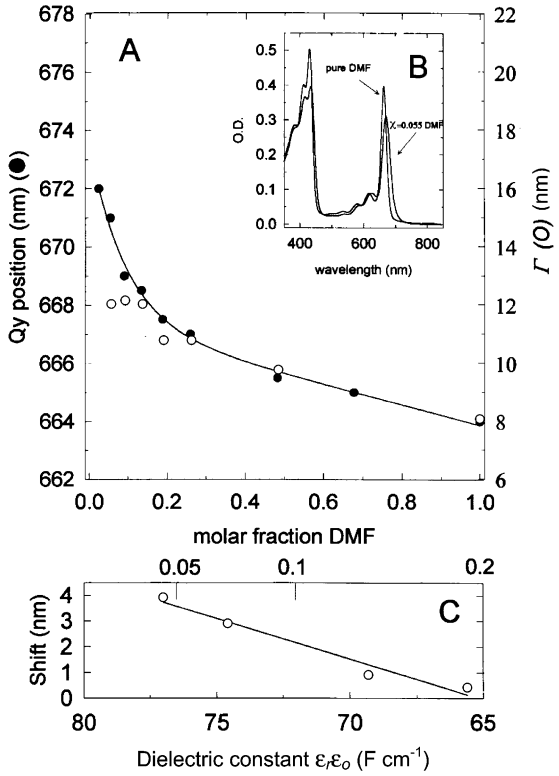

Figure 2. Dependence of peak position and relative fwhh/2 (Γ) on DMF mole fraction over the entire range of the binary mixture composition (panel A) for the Chl *a* Q_y transition. UV−vis spectra (panel B) of 5×10^{-6} M Chl *a* solution in pure DMF and in a solution at 0.055 DMF mole fraction. In panel C are shown the differences between the value of λ_{max} relative to DMF mole fractions ≤ 0.2.

which the pigment is present mainly as monomer, polymer, or micellar species, respectively.

Monomer. Chl *a* is virtually insoluble in water, where most of the associations investigated take place. This difficulty can be avoided by using an appreciable pigment concentration in a water miscible solvent and injecting an aliquot of such solution in the proper amount of water. Using this technique, the DMF-dissolved chlorophyll was added to water to form a set of solutions ranging over the entire mole fraction of the water−DMF mixtures. The UV−vis absorption spectra of these solutions were recorded immediately after the injection. In panel B of Figure 2, the spectrum corresponding to a 0.055 DMF mole fraction is compared to that of the same Chl *a* concentration in pure DMF. The increase of the water amount in the solution results in a red shift of ∼8 nm of the main peaks both in the red and in the blue regions and in an increase of the fwhh. As well-documented in the literature,[59] the observed changes are the result of bulk solvent effects, such as dielectric constant and refraction index and specific solute−solvent interactions.[33]

The dependence of the Q_y band position and of the fwhh on the DMF mole fraction over the entire range of the binary mixture in water is reported in panel A of Figure 2. The appearance of the spectral changes up to a DMF mole fraction of ∼0.2 could be interpreted as a gradual replacement of organic solvent molecules with water in key positions, such as the Mg atom, $^{13}C_1$═O carbonyl group, etc. The different interactions of the chlorophyll dipolar moment with the solvating molecules can be responsible for the broadening of the fwhh.[28,30] Once all of the coordinated molecules have been substituted, no further changes in the immediate vicinity of the pigment will take place and no further changes in the fwhh are expected. The value of mole fraction at which the influence of the solvent composition on the fwhh is completed marks the completion of the modifications in the chlorophyll coordination. Once this process has been concluded, the changes present in the spectra can be related to the bulk dielectric constant and refractive index that only slightly, if at all, influence the fwhh but strongly affect λ_{max}. In panel C of Figure 2, the differences between the value of λ_{max} relative to DMF mole fractions ≤ 0.2 are shown. The linear dependence of this difference on the solution dielectric constant further supports the above considerations.

Polymer. Figure 3 reports the spectra of 2×10^{-6} M Chl *a* recorded in four different organic solvents containing 70% (v:v) water and at different times from the sample preparation. The main feature of the spectra in acetone and ACN is the progressive growth of a long wavelength peak at 745 nm, which is completely absent in the spectra obtained in MeOH and DMF over the entire interval of Chl *a* concentration and time investigated. In DMF, no relevant changes of the absorbance are observed in time, whereas in the methanolic mixture, the chlorophyll gradually transforms in pheophytin (Pheo), as evidenced by the presence of the peaks at 410, 438, 507, and 538 nm[25] and by thin-layer chromatography. The nature of the 745 nm absorbing species has been extensively debated in the literature. On the basis of small-angle neutron scattering experiments,[66] the hypothesis of the formation of cylindrical reverse micelles, with a single water molecule cross-linking the magnesium, the keto, and the ester carbonyl group of neighboring chlorophylls, has been formulated. Alternatively, X-ray crystallographic structures of ethyl-chlorophyllide[14] reveal the presence of two water molecules involved in the bridge connecting the Mg atom and the ester carbonyl of one chlorophyll to the C-13 keto-group on a second pigment molecule. The presence of a strong conservative double band in the CD spectra[4,63] of this species is are consistent with the oligomeric structure formed by the repetition in the space of a dimeric minimal unity. A weak coupling between dimers was also invoked to explain the S-shaped CD spectrum of large bacteriochlorophyll olygomers.[21,55] The differences in water content and Chl *a* concentration necessary to the aggregates formation in different solvents have been previously interpreted in terms of solvation of hydrophobic solutes,[5,15] by evaluating the excess properties of the binary mixtures or the solution and transfer thermodynamic properties of hydrophobic solutes upon addition of water to the organic solvent. Several papers agree on the presence of various structural regions over the whole composition range of water−ACN mixtures.[10,17] At very low ACN mole fraction, below 0.2 (Figure 3), the solute molecules enter the water framework cavities without breaking their structure, and several excess properties maxima or minima, such as dielectric constant and viscosity, are observed. In this region, the dipole moment of ACN remains almost constant, whereas that of water strongly decreases. The hydrophobic effect and the high value of the dielectric constant can consequently account for Chl *a* aggregation, to minimize the interaction of the hydrophobic part of the molecule with water. The presence of hydrophobic interactions in the water rich region of acetone−water mixtures and the evidence that on the contrary, MeOH forms hydrogen bonds with water, thus participating to the water structure, can likewise explain the respective presence and absence of the Chl *a* polymer in these solvents.[8,35,36] Notwithstanding a strong hydrophobic effect, which has been reported in the literature for a water mole fraction 0.8,[52,67] similar considerations cannot be invoked to clarify the behavior of Chl

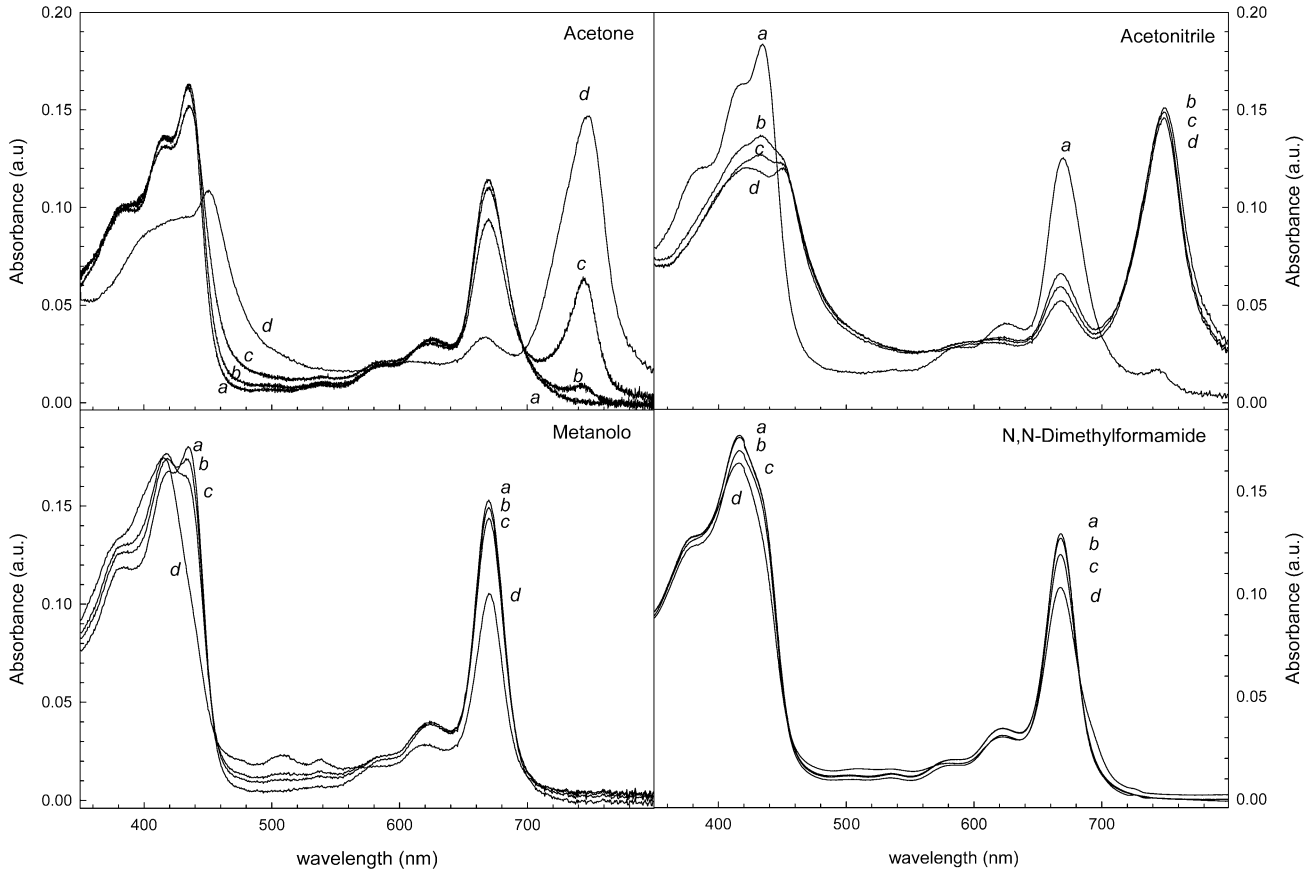

Figure 3. Absorption spectra of 2×10^{-6} M Chl *a* solutions in four different water−organic solvent binary mixtures at different times from sample preparation: (a) $t = 0$ h, (b) $t = 3$ h, (c) $t = 6$ h, and (d) $t = 24$ h. In all cases, the water content was 70% in volume.

TABLE 1: Donor Number,[22] Dielectric Constant,[38] and Dipolar Moment[38] of Water, Acetone, ACN, and DMF

solvent	donor no.	ϵ (F/cm)	μ (Debye)
H_2O	18.0	80.1	1.85
acetone	17.0	20.7	2.86
ACN	14.1	36.0	3.44
DMF	26.6	36.7	3.86

a in DMF, in which the polymer was never detected. The dielectric constant and dipole moment of DMF do not differ remarkably from those of ACN (see Table 1). On the other hand, we must consider that structural and spectroscopic Chl *a* behavior in solution are governed by intermolecular interactions based on the coordination to the Mg atom but also on the electric charges and Chl−Chl transition dipole, as well as by hydrogen bonds and electron−donor interactions involving the keto C═O groups.[34,57] Among the solvents under investigation, DMF represents the strongest ligand for Chl *a*, with a donor number of 26.6, whereas acetone and ACN act as weak ligands with donor numbers of 17.0 and 14.1, respectively.[61] DMF, therefore, even presenting the same coordination number of the other two solvents, has a stronger interaction with the pigment that can somehow contrast the hydrogen bonds formation between the water molecules, the Mg atom, and the C═O group of the chlorophyll, essential for the polymer formation.

Micellar Chl *a*. When the percentage of all of the organic solvents examined in water decreases below 10%, the main peak of the hydrated monomer at about 673 nm evolves toward a longer wavelength absorbing form, with maximum absorption at 713 nm. This species always forms in the different solvent examined, and its quantity depends on several factors such as nature of the solvent, Chl *a* concentration, organic solvent concentration, and time. In Figure 4, the absorption spectra of 2×10^{-5} M Chl *a* in DMF as a function of the organic solvent content are reported. At 1% DMF, the contemporary presence of the monomer peak and aggregated peak, at 673 and 713 nm, respectively, is observed. The dependence of the S713 formation on the organic solvent mole fraction is not trivial: its relative

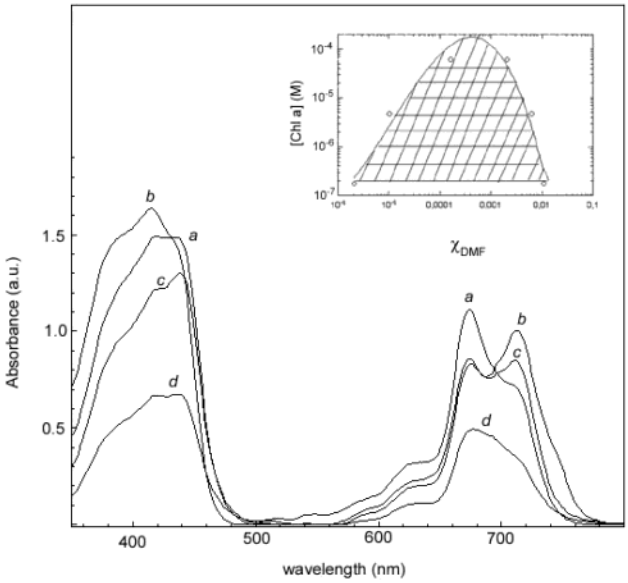

Figure 4. Absorption spectra of 2×10^{-5} M Chl *a* in DMF−water mixtures as a function of the organic solvent content. (a) $\chi = 0.002$, (b) $\chi = 0.001$, (c) $\chi = 0.0002$, and (d) $\chi = 0.00019$. Inset: S713 existence domain at various DMF−water solvent compositions and Chl *a* concentrations.

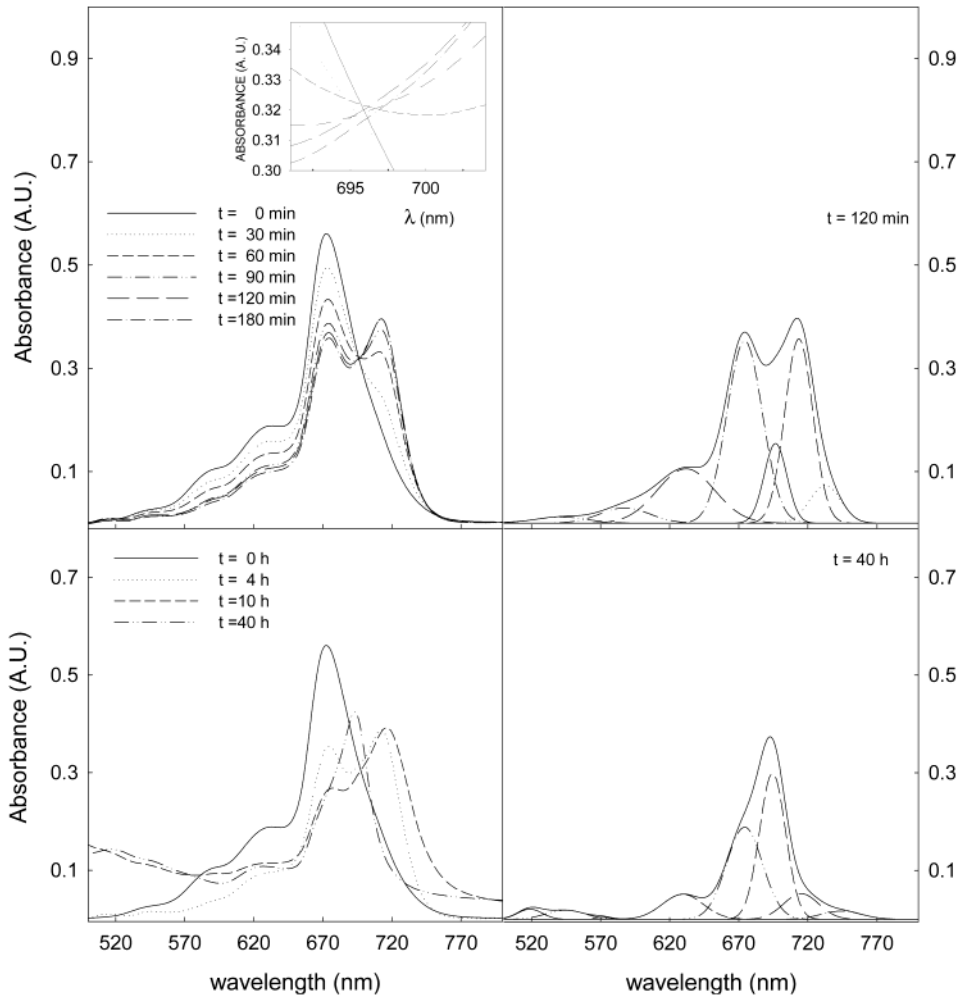

Figure 5. Time evolution of the red peak for a 7×10^{-6} M Chl *a* solution 0.0002 mole fraction of DMF in water in shorter (upper left) and longer (lower left) time intervals. The deconvolution of single spectra (right panels: 2 h (upper spectra) and 40 h (lower panel) from sample preparation) is performed as explained in the Material and Methods section. Peaks obtained from the deconvolution: (wavelength (nm)/fwhh (nm)): 756.2/95.5; 710.8/33.4; 693.1/19.9; 673.0/29.4; 631.0/48.7; and 592.3/32.7. Inset: enlargement of the wavelength interval 690−705 nm showing the crossing region of the peaks during the first 3 h from sample preparation.

intensity increases as compared to the monomer, when the content of organic solvent is lowered to a mole fraction of 0.001 whereas at smaller percentage of DMF it decreases, in favor of a new species absorbing at 696 nm (from now on called S696), as shown by the deconvolution procedures (see Figure 5). When DMF is below a mole fraction of 0.0002, a general decrease of the solution absorbance was observed due to a gradual precipitation of the chlorophyll. We can conclude that a limited range of the DMF−water composition exists where the S713 is formed. This range broadens on decreasing the Chl *a* concentration. The S713 existence domain at various solvent compositions and Chl *a* concentrations is summarized in the inset of Figure 4. For Chl *a* concentrations below 6×10^{-7} M and above 2×10^{-4} M, the S713 species was never detected at any value of the DMF−water ratio.

Figure 5 shows the time evolution of the red peak for a 7×10^{-6} M Chl *a* solution in water containing a mole fraction of 0.0002 of DMF, evidencing the gradual conversion of the Chl *a* monomer in the S713 species. The conversion reaches a maximum 120 min after sample preparation. The absence of a net isosbestic point in the conversion between the monomer and the S713 species, moreover, indicates that we are dealing with more than two equilibrating species in solution involved in the aggregation processes. Longer times result in the growth of the S696, which, after 40 h, becomes predominant in solution. In time, chlorophyll precipitation was also observed, clearly evidenced by the appearing of turbidity in solution, responsible for the increase of the spectral background at times longer than 4 h.

The spectral deconvolution (right part of the Figure 5) shows that the S696 is present in the spectra long before its appearing as a well-defined peak, competing with the growth of that at 713 nm.

The absorbance time evolution for the three peaks involved in the Chl *a* aggregation processes is shown in Figure 6. In the first 160 min, a decreasing of the monomer peak, together with the increasing of the S713 absorbance, is observed, while the S696 remains substantially unaltered. After this elapsed time, a general decreasing of the absorbance is observed, due to precipitation processes. After 1200 min, a subsequent transformation between the species takes place; the S696 starts to increase, becoming the main species in solution, to the detriment of S713. In the inset of the same Figure, the data referred to a shorter time interval are reported. To make clearer the correlation between the transforming species, in the inset, the absorbance is reported as the difference between the actual value and A_0, the initial value relative to each species calculated from the deconvolution procedure. It is evident that S696, present since the beginning in solution, does not remarkably change its concentration in the first 160 min during the monomer trans-

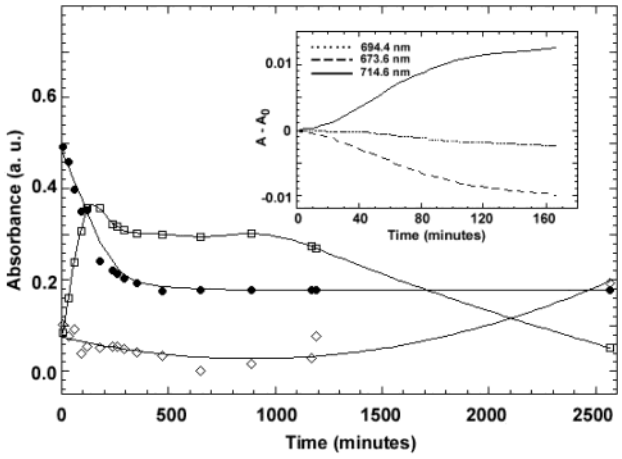

Figure 6. Time evolution for the three peaks in the red region involved in the Chl *a* aggregation processes. Monomer (filled circles), S713 (empty squares), and S696 (empty diamonds). In the inset, the data that referred to a shorter time interval are reported. The absorbance in the inset is expressed as differences between absorbance in time and the initial value A_0 relative to each species, obtained from spectral deconvolution.

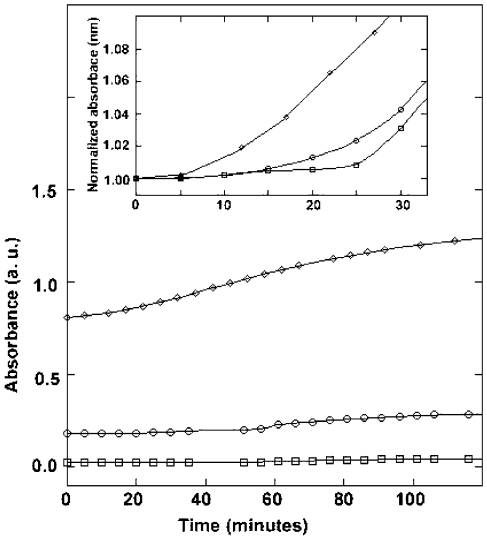

Figure 7. Time course of S713 formation at different bulk Chl *a* concentrations. In the inset, the data that referred to a shorter time interval are reported. The data were obtained from the deconvolution procedures.

formation in S713. The growth of the S713 absorbance, mirrored by the decrease of the signal at 674 nm, shows a sigmoidal feature. The time elapsed from the sample preparation and the aggregate formation, i.e., "lag time", decreases with increasing the bulk Chl *a* concentration (see Figure 7). Sigmoidal build-up curves, characterized by the presence of an induction period before the aggregation processes, have been recently reported by Balaban et al.[7] for the kinetics of formation of chlorosomal aggregates of Chlorophyll *c*. In literature, similar behaviors are well-documented for self-aggregation processes of other large biomolecules. In these cases also, an autocatalytic mechanism of growth of larger aggregates from a "critical" nucleus[16,37,47,46,49−51] has been proposed. The relative slowness of the S713 formation and the decrease of the induction time with the increase of the Chl *a* concentration are consistent with a model of nuclei growth at the expenses of monomers, which usually has been used to describe the formation of crystals and colloidal particles. The critical size of the aggregate in equilibrium with the monomer is inversely proportional to the monomer concentration: at high Chl *a* concentration, even small particles tend to increase their size. Conversely, at low bulk concentration, the critical size is large, and aggregates smaller than this size will have the tendency to dissolve. Recently, Pasternack et al.[49] proposed a nonconventional approach to analyze the formation kinetics of different supramolecular assemblies. The reported rate law is given by the following expression:

$$-\frac{\mathrm{d[M]}}{\mathrm{d}t} = k(t)\left\{\frac{([\mathrm{M}] - [\mathrm{M}]_e)^m}{([\mathrm{M}]_0 - [\mathrm{M}]_e)^{m-1}}\right\} \qquad (1)$$

where m is an index related to the number of monomers in the initial nucleus; [M], $[M]_0$, and $[M]_e$ are the concentration of monomeric units at the time t, at the beginning of the process and after attainment of equilibrium, respectively. Upon occurrence of autocatalysis, the rate constant $k(t)$ is time-dependent, and it is expressed as $k(t) = k_0 + k_c(k_c \cdot t)^n$. The rate constant k_0 refers to the process in the absence of catalyst, while the k_c constant is related to the autocatalytic pathway. The exponent n derives from the theory of self-similar aggregation, in which the size of aggregates scales with the time according to a power law.[43] The analysis of our kinetic traces ([Chl *a*] = 1.9−60 μM) according to this equation gave a good quality of the fit (Figure 1, Supporting Information).

The values of the noncatalytic rate constant k_0 are about 10^{-4} s^{-1}, while the values of the catalytic rate seem to be independent of the initial chlorophyll concentration and range at about 3.5 ($\pm$0.7) $\times$ 10^{-4} s^{-1}. This observation is in contrast with the analysis of other porphyrin aggregating systems (e.g., formation of J-aggregates of diacid tetrakis(4-sulfonatophenyl)porphine), in which the k_c rates depend on the initial conditions, i.e., the concentration of porphyrin. The values of the parameters m and n obtained for a series of kinetic analyses in the case of Chl *a* are in the range of 1.8 $\pm$ 0.5 and 1.3 $\pm$ 0.2, respectively. The m values seem to indicate that the basic aggregative process begins with monomers or dimers.

The S713 has been observed as a Chl *a* aggregation product in several aqueous mixtures in the presence of organic solvent such as MeOH, ACN, dioxane, and dimethyl sulfoxide. Its structure can be hypothesized as an aggregate in which the phytil chains of the Chl *a* are surrounded by the organic solvent and the macrocyclic heads are displayed toward the water bulk.[6] An alternative hypothesis is based on a T-shaped oligomer, whose molecules are loosely coupled to each other, and their aggregation is stabilized by hydrophobic effects.[44] A peak at 713 nm, together with a shoulder at 696 nm, was indeed observed for Chl *a*′ in aqueous MeOH and attributed to a T-shaped precursor evolving toward an aggregate composed of many stacked macrocycles.[45]

On these bases, further investigations were undertaken by using independent techniques able to provide complementary information on the size and nature of the different species involved in the interconversion processes reported in Figures 6 and 7.

Figure 8 reports the voltammograms of a solution 1×10^{-5} M Chl *a* in a mole fraction of 0.0002 DMF, after 1 min adsorption on the HMDE. The continuous curve was obtained immediately after a Chl *a* injection, when only the monomer was present, while the dotted one was recorded once the S713 species was formed in solution. Both voltammograms evidence the signals relative to the reduction of the carbonyl group at −660 mV and those relative to the formation of Chl *a* radical anion and dianion at −1041 and −1395 mV, respectively.[29]

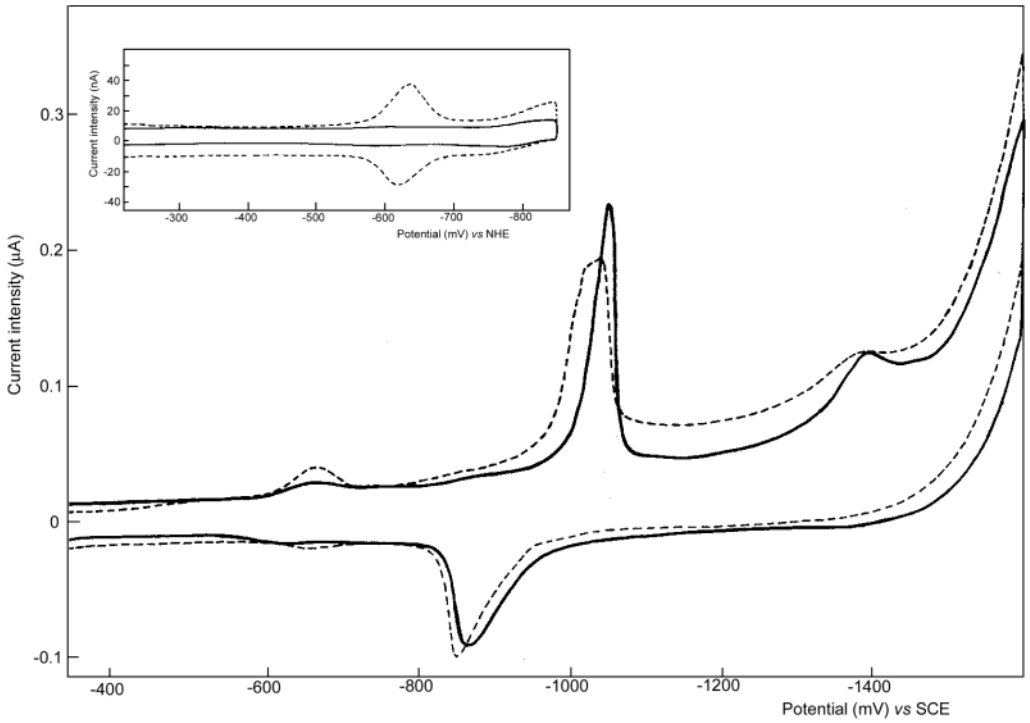

Figure 8. Voltammograms of Chl *a* 1×10^{-5} M solution 0.0002 mole fraction of DMF in water. Experimental conditions are described in the Material and Methods. The continuous curve was recorded immediately after Chl *a* injection while the dotted curve was recorded once the S713 was formed in solution.

Significantly, the presence of the aggregate absorbing at 713 nm results in a noticeable enhancement of the electrochemical peak at −660 mV, relative to the reduction of the C═O group.[29] This finding is even more evident in the data, collected in a reduced potential range in order to avoid the reduction of the porphyrin ring, and reported in the figure inset. The increase of the carbonyl reduction signal in the sample containing the S713 can be attributed to a structural organization in which the C═O groups are oriented toward the external bulk water solution, thus favoring the preferential adsorption of the molecule on the mercury surface through them. On the other side, the almost complete disappearance of the second reduction wave suggests the staking of the porphyrin macrocycles, which prevents the reduction of the ring at the electrode.

Figure 9 shows the CD spectra of Chl *a* solutions in a mole fraction of 0.0002 of DMF in water recorded at different times from the sample preparation. As expected,[18,65] freshly prepared samples containing the monomer as prevalent species do not evidence any significant signal, despite the presence of three chiral centers on the molecule. A conservative double band with zero crossing at 720 nm, a negative peak at 730 nm, and a positive peak at 715 nm appears when the sample contains the S713, indicative of coupling between the dipole transition of different molecules of the aggregate. Significantly, the gradual replacement of the 713 nm peak by the 696 one, in the absorption spectra of Figure 5, is accompanied by relevant changes in the CD spectra: an inversion in the sign of the conservative signal is evident, together with its shift to higher energies. After 24 h, a negative Cotton effect is detected, with zero crossing at 695 nm.

RLS is an extremely sensitive and selective technique to detect chromophore aggregation.[42,48] RLS phenomenon arises from an enhancement of the scattered light intensity in the red edge portion of an absorption band, allowing for the specific identification of aggregated chromophores, even in complex matrixes.[11,39,40] The conditions to be met for observing this effect

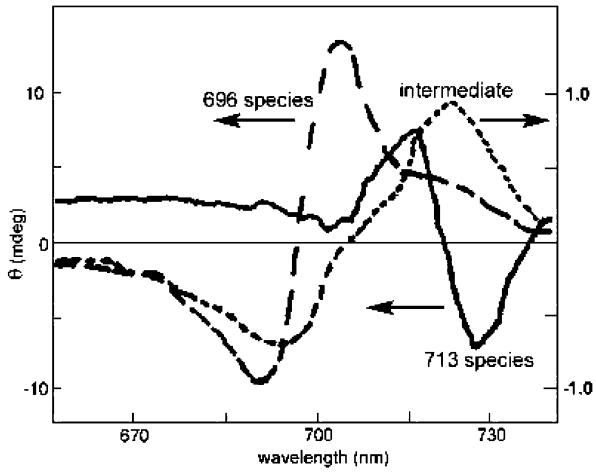

Figure 9. CD spectra of 5×10^{-5} M Chl *a* solutions in a mole fraction of 0.0002 of DMF in water recorded at different times from the sample preparation. Spectra 2 h (—), 24 h (- - -), and 48 h (− − −) from sample preparation. The presence of the different species has been checked by the corresponding absorption spectra.

are (i) a strong electronic coupling between adjacent chromophores, (ii) large size and proper geometry of the resulting aggregate (for aggregated porphyrins and chlorophylls a minimum aggregation number of 25 monomers has been estimated),[46] and (iii) intense molar absorbance of the monomeric unit.[48] These requirements are fulfilled by the aggregated Chl *a*, in which the interacting chromophores exhibit large molar extinction coefficients and the size of the aggregate, as measured by DLS (see below), indicates the presence of a large number of monomeric units.

A simple quantum mechanical model for RLS, based on exciton-coupling theory, has been recently reported, addressing the relationship between the intensities of the observed RLS features and the electronic and geometrical properties of the aggregates.[46]

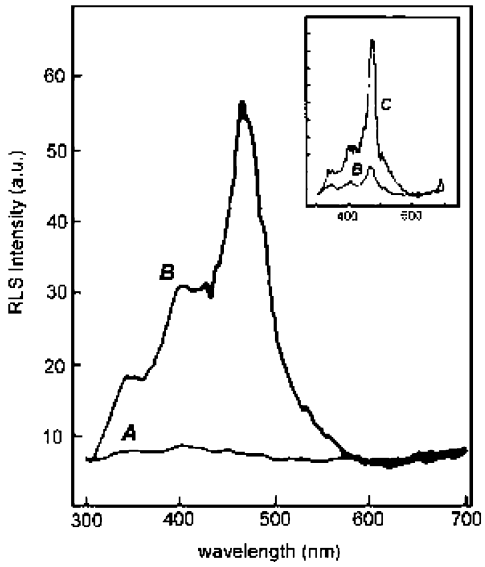

Figure 10. RLS profiles of the different species of Chl *a* in 0.1% DMF in water: monomer (curve A) and S713 species (curve B). In the inset, the curve A is compared with the RLS signal relative to the 745 nm absorbing polymer (curve C) prepared in ACN as in Figure 2.

Figure 10 shows the RLS profiles of the different species of Chl *a* in 0.1% DMF in water. The solution containing the monomer (curve a) does evidence a very weak scattering intensity. A strong signal in the region between 400 and 500 nm, indicative of large aggregates with strong excitonic coupling between the chromophores, was observed when the concentration of the S713 reached its maximum value in solution. Dynamical properties of species in solution can be obtained by quasi-elastic light scattering. In particular, the photon correlation spectroscopy technique allows for investigating the dynamics of aggregates through the measurement of the normalized autocorrelation function of the scattered intensity $I_s(k,t)$:[9]

$$g_2(k,t) = \frac{\langle I_S(k,0)\, I_S(k,t)\rangle}{\langle I_S(0)\rangle^2}$$

where k is the exchanged wavevector. If the scattered field obeys Gaussian statistics, the Siegert's relation can be applied[9]

$$g_2(k,t) = 1 + \alpha|g_1(k,t)|^2$$

where α is a constant depending on the experimental setup and $g_1(k,t)$ is the normalized field autocorrelation function.

For diffusing monodispersed spherical objects, the intensity correlation function decays exponentially, according to $g_2(k,t) = 1 + \alpha \exp(-2\Gamma t)$. For homogeneous, Euclidean, noninteracting monodispersed spheres, under the fulfillment that $k_R \ll 1$, $\Gamma = D_C k^2$, where D_C is the collective translation diffusion coefficient, which gives information on the hydrodynamic radius through the Einstein−Stokes relation $R_H = k_B T/6\pi\eta D_C$, with η the solvent viscosity and k_B the Boltzmann constant.[9] R_H is an "effective" size, depending on the hydrodynamic interactions with the solvent and on the interparticle interactions.

Under the condition $kR \gg 1$, the k_2 dependence of the relaxation rate Γ loses validity, because of the sensitivity of light scattering to particle internal motions. If the diffusing objects are rigid and monodispersed, the k_2 dependence and the Einstein−Stokes relation are still valid.[9]

The diffusion coefficients of the aggregated species have been measured under the same experimental conditions by DLS. The corresponding hydrodynamic radii have been estimated at about 20 nm, assuming the Stokes−Einstein equation. The values of the diffusion coefficients do not depend on the exchanged wavevector, suggesting that actually they refer to traslational motion of the particles. Both the concentration and the size of these clusters, which can be detected immediately after sample preparation, increased in time. The macroscopic feature of these aggregates was observed by low resolution TEM, which confirmed (see Figure 11) the presence of spherical particles of about 15 nm of diameter, together with 10 times larger spherical clusters of particles, randomly formed in different areas of the sample.

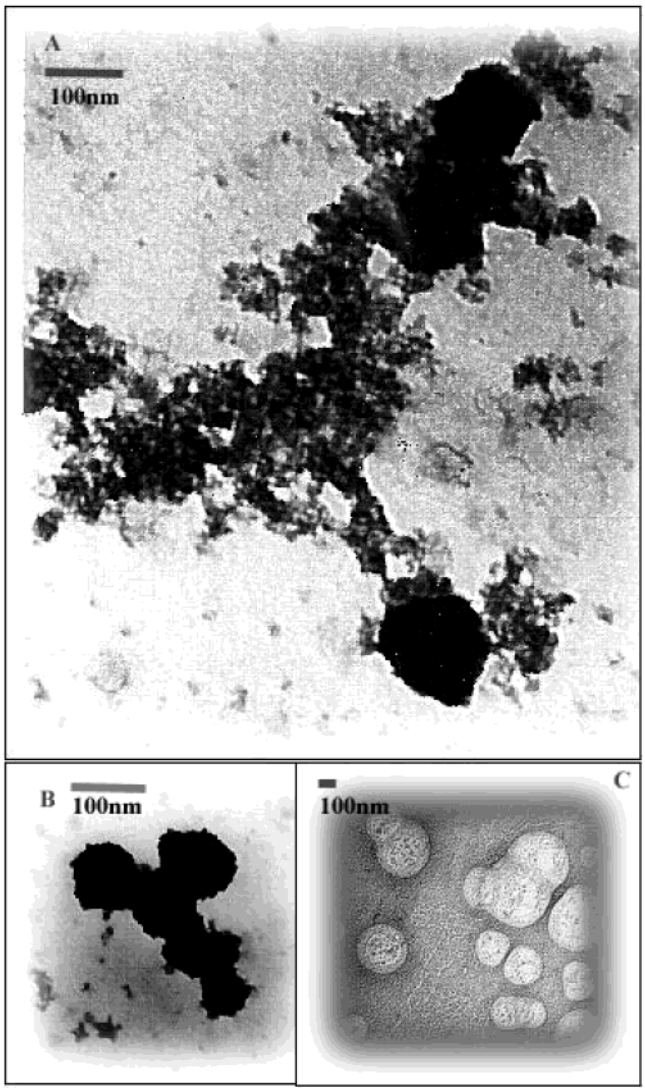

Figure 11. Low-resolution TEM of macroscopic aggregate S713. The three micrographs are relative to different areas of the sample and different instrumental resolution.

The overall data above-reported are consistent with the attribution of the S713 species to a spherical-shaped aggregate originated by aggregation of chlorophyll molecules and in which the phytil chains are segregated in the inner part, thus fostering the pigments to expose the macrocyclic heads toward the bulk water solvent. The role of DMF in the formation of this aggregate has been investigated by measuring the organic solvent self-diffusion coefficient D using FT-PGSE NMR techniques. The confinement of the organic solvent in the core of the Chl *a* micelle would result in a substantial decrease of the diffusion coefficient as compared to the free organic solvent,

due to the aggregate slow diffusion. The DMF self-diffusion coefficient measurements were carried out on different samples at various organic solvent percentage keeping at 1×10^{-5} M the value of the Chl *a* concentration. The invariance of the measured value ($D \cong 1 \times 10^{-9}$ m^2/s) on the experimental conditions supports the hypothesis that the role of DMF is only limited to transfer the Chl *a* into the aqueous solution, without being confined inside the micelle. The high hydrophobic effect, on the contrary, induces the Chl *a* molecules to self-organize in order to minimize the water−phytil chains repulsive interactions, leading to closed structures, similar to liposomes. The growth of these species was accompanied by a decrease of fluorescence intensity, confirming the presence of pigment−pigment interactions, which are responsible for quenching of the emission signal through intramolecular energy transfer. The driving force for this spontaneous process could be given by the negative enthalpic contribution to the S713 formation. Furthermore, the increase of the entropic content of water, mainly due to a Chl *a* self-aggregation process, could play an important role. The colloidal nature of the S713 aggregate is further supported by data recorded after the addition of small amounts of concentrated KCl solutions to samples where this species was already present. The UV−vis spectra show a gradual shift of the absorption to longer wavelengths evidencing the formation of the polymeric species. The polymer is also evidenced in the RLS spectra (see inset of Figure 10), by the presence of a more structured and intense peak in comparison to that relative to the S713. Besides DLS, measurements conducted on these samples showed features typical of fractal aggregates. These structural changes can be all retraced to a destabilizing process in colloidal systems due to the screening effects determined by strong electrolytes.

The DLS analysis was also conducted on samples after the conversion to S696. Remarkably, the diffusion coefficients resulted to be again independent of the scattering wavevector, and the corresponding hydrodynamic radii were very similar to those previously calculated for the 713. The idea of a smaller aggregate was therefore excluded, and the investigations on this species were oriented toward demetalation processes of the chlorophylls. In Figure 12, UV−vis, CD, and RLS spectra of a solution of Pheo in water containing a mole fraction of 0.0002 of DMF are reported. In time, the formation of the S696 nm was observed, whose CD and RLS spectra are closely similar to those recorded under the same conditions for Chl *a* after 24 h from the preparation. In particular, the RLS profile evidences an intense peak around 470 nm, and a weaker one centered at 705 nm. This latter feature can be assigned to RLS effect arising from the Q-band at 696 nm. De Paula et al.[16] reported a weak RLS feature at 699 nm in the case of Chl *a* aggregates in 9:1 formamide:water mixture. The presence of a fluorescence contribution can be excluded, as emission is almost completely quenched by aggregation.

The loss of the central Mg ion, probably due to a pH decrease in the internal part of the aggregate or to steric costraints of the macrocycles, does not imply the destruction of the supramolecular organization. The demetalation only induces a change in the relative orientation of the carbonyl group of Chl *a* molecules, accounting for the opposite sign of the Cotton effect.

Because Pheo *a* lacks the Mg ion, which is required for hydrogen bonding between water and different Chl *a* molecules, it seems reasonable to assume that the above-reported supramolecular self-aggregation processes in the water rich region are predominantly driven by the strong hydrophobic effect due to the phytil chain. The consideration that spectra of solutions

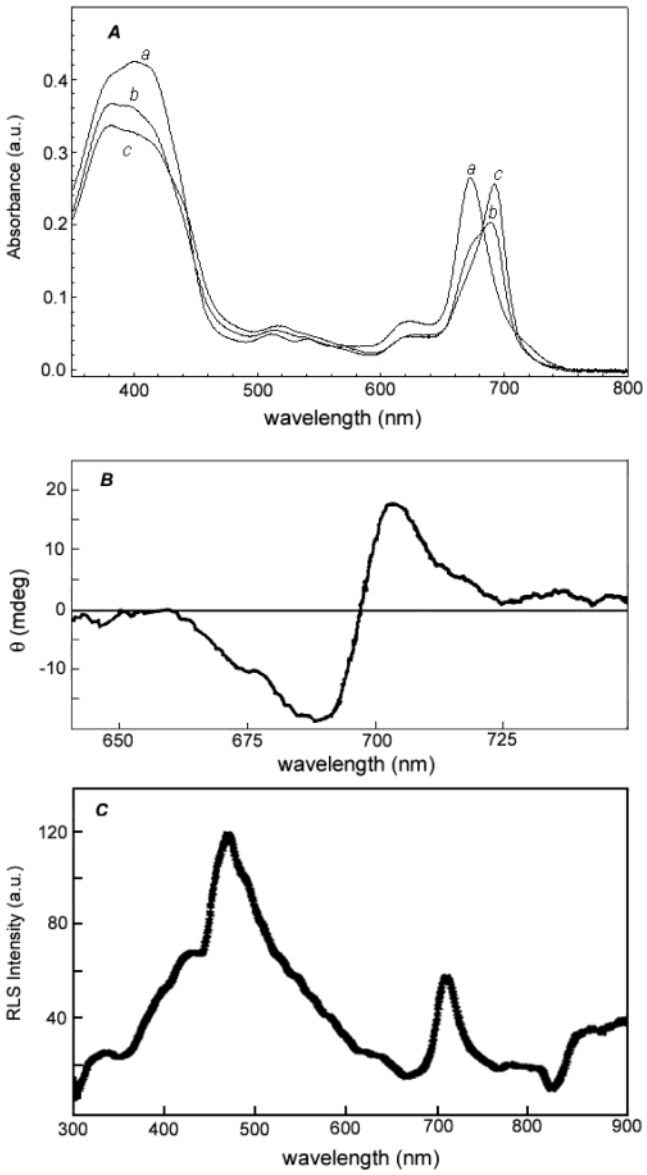

Figure 12. UV−vis (panel A), CD (panel B), and RLS (panel C) spectra of a Pheo solution in a mole fraction of 0.0002 DMF in water. The UV−vis spectra were recorded immediately (curve a), 2 h (curve b), and 24 h after sample preparation (curve c). The CD and RLS spectra were recorded at 24 h.

containing the S696 are very similar to that reported for synthetic Chl *a* dimers[12,27] in which the two pigments are covalently linked through the side chains strongly supports this hypothesis.

Acknowledgment. We thank Dr. Teresa Bleva (CNR-Bari) for the TEM images of the chlorophyll aggregates shown in Figure 11.

Supporting Information Available: Kinetic profile of the absorbance at 713 nm. This material is available free of charge via the Internet at http://pubs.acs.org.

References and Notes

(1) Agostiano, A. *J. Photochem. Photobiol. A* **1993**, *17*, 293.
(2) Agostiano, A.; Butcher, K. A.; Showell, M. S.; Gotch, A. J.; Fong, F. K. *Chem. Phys. Lett.* **1987**, *137*, 37.
(3) Agostiano, A.; Catucci, L.; Colafemmina, G.; Della Monica, M.; Scheer, H. *Biophys. Chem*. **2000**, *84*, 189.
(4) Agostiano, A.; Catucci, L.; Colafemmina, G.; Scheer, H. *J. Phys. Chem. B* **2002**, *106*, 1446.

(5) Agostiano, A.; Cosma, P.; Della Monica, M.; Fong, F. K. *Bioelectrochem. Bioenerg.* **1990**, *23*, 311.
(6) Agostiano, A.; Della Monica, M.; Palazzo, G.; Trotta, M. *Biophys. Chem.* **1993**, *47*, 193.
(7) Balaban, T. S.; Leitich, J.; Holzwarth, A. R.; Schaffner, K. *J. Phys. Chem. B* **2000**, *104*, 1362.
(8) Bergstrom, S.; Oloffson, G. *J. Solution Chem.* **1978**, *7*, 497.
(9) Berne, B. J. In *Dynamic Light Scattering with Application to Chemistry, Biology and Physics*; Pecora, R., Ed.; J. Wiley and Sons: New York, 1976.
(10) Bertie, J. E.; Lan, Z. *J. Phys. Chem. B* **1997**, *101*, 4111.
(11) Borissevitch, I. E.; Tominaga, T. T.; Imasato, H.; Tabak, M. *Anal. Chim. Acta* **1997**, *343*, 281.
(12) Boxer, S. G.; Closs, G. L. *J. Am. Chem. Soc.* **1976**, *98*, 6.
(13) Chauvet, J. P.; Viovy, R.; Santus, R.; Land, E. J. *J. Phys. Chem.* **1981**, *85*, 3449.
(14) Chow, H. C.; Serlin, R.; Strouse, C. E. *J. Am. Chem. Soc.* **1975**, *97*, 7230.
(15) Cosma, P.; Agostiano, A.; Catucci, L.; Ceglie, A.; Colafemmina, G.; Mallardi, A.; Palazzo, G.; Trotta, M.; Della Monica, M. In *Properties and Chemistry of Biomolecular Systems*; N. R., Ed.; Kluwer Academic: Dordrecth, 1994; p 159.
(16) dePaula, J. H.; Roblee, J. H.; Pasternack, R. F. *Biophys. J.* **1995**, *68*, 335.
(17) Easteal, A. J.; Woolf, L. A. *J. Chem. Thermodyn.* **1988**, *20*, 702.
(18) Fidler, V.; Osborne, A. D. *J. Chem. Soc., Chem. Commun.* **1980**, 1056.
(19) Fong, F. K.; Showell, M. S.; Alfano, A. J. *J. Am. Chem. Soc.* **1985**, *107*, 765.
(20) Fong, F. K.; Showell, M. S.; Alfano, A. J. *J. Am. Chem. Soc.* **1985**, *107*, 7231.
(21) Gotistein, J.; Scheer, H. *Proc. Natl. Acad. Sci. U.S.A.* **1983**, *80*, 2231.
(22) Gutmann, V. *Coord. Chem. Rev.* **1976**, *18*, 225−255.
(23) Haran, G.; Wynne, K.; Moser, C. C.; Dutton, P. L.; Hochstrasser, R. M. *J. Phys. Chem.* **1996**, *100*, 17076.
(24) Hiller, R. G.; Anderson, J. M.; Larkum, A. W. D. In *Chlorophylls*; Scheer, H., Ed.; CRC Press: Boca Raton, FL, 1991; p 529.
(25) Hoff, A. J.; Amesz, J. In *Chlorophylls*; Scheer, H., Ed.; CRC Press: Boca Raton, FL, 1991; p 723.
(26) Hoshino, M.; Inamura, N.; Koike, K.; Kikuki, K.; Kokubun, H. *Photochem. Photobiol.* **1983**, *38*, 225.
(27) Huang, C. Z.; Li, K. A.; Tong, S. Y. *Anal. Chem.* **1997**, *69*, 514.
(28) Hynninen, P. H.; Lötjönen, S. *Biochim. Biophys. Acta* **1993**, *1183*, 381.
(29) Kanova, L. A.; Tarasevich, M. R. *J. Electroanal. Chem.* **1987**, *227*, 99.
(30) Katz, J. J.; Shipman, L. L.; Cotton, T. M.; Janson, T. R. In *The Phorphyrins Physical Chemistry Part C*; Dolphin, D., Ed.; Academic Press: New York, 1978; Vol. V, p 402.
(31) Kimaier, C.; Holten, D. *Photosynth. Res.* **1987**, *13*, 225.
(32) Kimaier, C.; Holten, D. In *The Photosynthetic Reaction Center*; Deisenhofer, J., Norris, J. R., Eds.; Academic Press: San Diego, 1993; Vol. 2, p 49.
(33) Koyama, Y.; Limantara, L. *Specrochim. Acta* **1988**, *54A*, 1127.
(34) Krawczyk, S. *Biochim. Biophys. Acta* **1989**, *140*, 149.
(35) Laaksonen, A.; Kusalik, P. G.; Svishchev, I. M. *J. Phys. Chem. B* **1997**, *101*, 5910.
(36) Lara, J.; Desnoyeres, J. E. *J. Solution Chem.* **1981**, *10*, 465.
(37) Leyvraz, F. In *On Growth and Form*; Stanley, H. E., Ostrowsky, N., Eds.; Martinus Nijhoff Publishers: Dordrecht, 1986.
(38) Lide, D. R. *Handbook of Chemistry and Physics*, 77th ed.; CRC Press: Boca Raton, FL, 1996.
(39) Ma, C. Q.; Li, K. A.; Tong, S. Y. *Anal. Biochem.* **1996**, *239*, 86.
(40) Ma, C. Q.; Li, K. A.; Tong, S. Y. *Fresenius J. Anal. Chem.* **1997**, *357*, 915.
(41) Maly, P.; Danielius, R.; Godonas, R. *Photochem. Photobiol.* **1987**, *45*, 7.
(42) Micali, N.; Romeo, A.; Lauceri, R.; Purrello, R.; Mallamace, F.; Monsù-Scolaro, L. *J. Phys. Chem. B* **2000**, *104*, 9417.
(43) Norris, J. R.; Scheer, H.; Kats, J. J. *Ann. N. Y. Acad. Sci.* **1974**, *244*, 260.
(44) Oba, T.; Furukawa, H.; Wang, Z. Y.; Nozawa, T.; Mimuro, M.; Tamiaky, H.; Watanabe, T. *J. Phys. Chem. B* **1998**, *102*, 7882.
(45) Oba, T.; Wang, Z. Y.; Nozawa, T.; Mimuro, M.; Yoshida, S.; Watanabe, T. *J. Phys. Chem. B* **1997**, *101*, 3261.
(46) Parkash, J.; Robblee, J. H.; Agnew, J.; Gibbs, E. J.; Collings, P. J.; Pasternack, R. F.; dePaula, J. C. *Biophys. J.* **1998**, *74*, 2089.
(47) Pasternack, R. F.; Bustamante, C.; Collings, P. J.; Giannetto, A.; Gibbs, E. J. *J. Am. Chem. Soc.* **1993**, *115*, 5393.
(48) Pasternack, R. F.; Collings, P. J. *Science* **1995**, *269*, 935.
(49) Pasternack, R. F.; Ewen, S.; Rao, A.; Meyer, A. S.; Freedman, M. A. *Inorg. Chim. Acta* **2001**, *317*, 59.
(50) Pasternack, R. F.; Fleming, C.; Herring, S.; Collings, P. J.; dePaula, J.; DeCastro, G.; Gibbs, E. J. *Biophys. J.* **2000**, *79*, 550.
(51) Pasternack, R. F.; Gibbs, E. J.; Collings, P. J.; De Paula, J. H.; Turzo, L. C.; Terracina, A. *J. Am. Chem. Soc.* **1998**, *120*, 5837.
(52) Rouw, A. C.; Somùsen, G. *J. Solution Chem.* **1981**, *10*, 533.
(53) Scheer, H. In *Chlorophylls*; Scheer, H., Ed.; CRC Press: Boca Raton, FL, 1991; p 3.
(54) Scheer, H.; Katz, J. J. *J. Am. Chem. Soc.* **1978**, *100*, 561.
(55) Scherz, A.; Rosembach-Belkin, V. *Proc. Natl. Acad. Sci. U.S.A.* **1989**, *86*, 1505.
(56) Scherz, A.; Rosenbach-Belkin, V.; Fisher, J. R. E. *Proc. Natl. Acad. Sci. U.S.A.* **1990**, *87*, 5430.
(57) Seely, G. R.; Jensen, R. G. *Spectrochim. Acta* **1965**, *21*.
(58) Sprague, S. G.; Varga, A. R. Membrane Architecture of Anoxygenic Photosynthetic Bacteria. In *Photosynthesis III: Photosynthetic Membranes and Light Harvesting Systems*; Staehelin, L. A., Arntzen, C. J., Eds.; Springer-Verlag: New York, 1986; Vol. 19.
(59) Stern, E. S.; Timmons, C. J. *Gillam and Stern's Intoduction to Electronic Absorption Spectroscopy in Organic Chemistry*; E. Arnold Ltd.: London, 1970.
(60) Strain, H. H.; Thomas, M. R.; Katz, J. J. *Biochim. Biophys. Acta* **1963**, *75*, 306.
(61) Umetsu, M.; Yu-Wang, Z.; Kobayashi, M.; Nozawa, T. *Biochim. Biophys. Acta* **1999**, *1410*, 19.
(62) Vladkova, R. *Photochem. Photobiol.* **2000**, *71*, 71−83.
(63) Volkov, A. G.; Gugsehashvili, M. I.; Kandelaki, M. D.; Markin, V. S.; Zelint, B.; Munger, G.; Leblanc, M. R. *Photochem. Photoelectrochem. Org. Inorg. Mol. Thin Films* **1991**, 1436.
(64) Vos, M. H.; Breton, J.; Martin, J. L. *J. Phys. Chem. B* **1997**, *101*, 9820.
(65) Wolf, H.; Scheer, H. *Ann. N. Y. Acad. Sci.* **1973**, *206*, 549.
(66) Worcester, D. L.; Michalski, T. J.; J. J., K. *Proc. Natl. Acad. Sci. U.S.A.* **1986**, *83*, 37961.
(67) Zielkiewicz, J. *J. Phys. Chem.* **1995**, *99*, 4787.